T7 RNA Polymerase-Induced Bending of Promoter DNA Is Coupled to DNA Opening†

Guo-Qing Tang and Smita S. Patel*

Department of Biochemistry, University of Medicine and Dentistry of New Jersey-Robert Wood Johnson Medical School, 675 Hoes Lane, Piscataway, New Jersey 08854

Received November 8, 2005; Revised Manuscript Received February 27, 2006

ABSTRACT: To initiate transcription, T7 RNA polymerase (RNAP) forms a specific complex with its promoter DNA and melts several base pairs near the initiation site to form an open complex. Previous gel electrophoresis studies have indicated that the promoter DNA in the initiation complex is bent [Ujvari, A., and Martin, C. T. (2000) *J. Mol. Biol. 295*, 1173−1184]. Here we use fluorescence resonance energy transfer (FRET) to investigate the conformation of promoter DNA in the closed and open complexes of T7 RNAP. We have used steady state and time-resolved fluorescence approaches to measure the FRET efficiency in a doubly dye-labeled duplex promoter and in a premelted bubble promoter. Changes in the FRET efficiency and hence the DNA end-to-end distance changes are small when the duplex promoter forms a complex with T7 RNAP. On the other hand, FRET changes are relatively larger when the bubble promoter binds T7 RNAP or when initiating nucleotides are added to the duplex promoter−T7 RNAP complex. The shortening of DNA end-to-end distances is indicative of DNA bending in the bubble DNA complex and in the duplex promoter complex with the initiating nucleotides. Our results are consistent with the model in which in the absence of initiating nucleotides there is a distribution of closed and open complexes, and the promoter DNA is bent slightly by $<40°$ in the closed complex but bent more sharply by 86° in the open complex. The energetics of DNA bending suggests that a significant part of the available free energy from promoter and polymerase interactions is utilized in DNA bending and/or untwisting. We propose that promoter opening occurs spontaneously upon DNA bending and/or untwisting as free energy is gained through interactions of the melted promoter with the T7 RNAP active site.

Promoter DNA bending induced by RNA polymerase (RNAP)[1] binding has been observed in phage (*1*−*3*), bacteria (*4*, *5*), yeast mitochondria (*6*), and eukaryotic RNAP systems (*7*, *8*). In *Escherichia coli* RNAP, the bending angle of the promoter DNA characterized ranged from $\leq 45°$ to 45−70° depending on the methods used to measure the bending angle (*4*, *9*−*11*). In bacteriophage T7 RNAP, gel electrophoresis analysis of the initiation complexes with DNA fragments containing the T7 promoter consensus sequence indicated a ∼40−60° bend in the promoter DNA centered around the start site of transcription initiation (*1*). On the other hand, modeling studies of a longer DNA into the crystal structure of the ternary initiation complex of T7 RNAP suggested an overall bend of ∼80° in the promoter centered around the transcription start site and unwinding of the downstream DNA by 146° (*3*).

Kinetic studies of promoter DNA binding have indicated that open complex formation in T7 RNAP occurs via a kinetic intermediate (*12*, *13*). On the basis of 2-AP fluorescence studies and the effects of initiating nucleotides, we proposed that this kinetic intermediate is likely the closed complex in which the DNA base pairs are not melted. Both $KMnO_4$ modification and fluorescence studies indicated that only 15−30% of the RNAP−DNA initiation complexes with the duplex promoter are fully open in the absence of the initiating nucleotides (*12*, *14*). Thus, a majority of the T7 RNAP−promoter DNA complexes during initiation are closed rather than open. Binding of the initiating nucleotides drives the conversion of the closed complexes to the open complexes (*13*, *15*, *16*). The crystal structures of T7 RNAP initiation complex have provided the structure of the promoter DNA in the open complex (*17*, *18*), but the structure of the DNA in the closed complex is unknown. Here we have investigated the properties of the DNA in the closed and open complexes and determined whether T7 RNAP bends the promoter DNA equally or differently in these complexes.

The structure of T7 promoter DNA in the initiation complexes was studied using the method of fluorescence resonance energy transfer (FRET). FRET studies have been used to determine distances, to characterize DNA bending, and to study the effect of nucleic acid sequence or protein binding on DNA bending (*19*−*23*). We labeled a T7 promoter DNA fragment with Alexa-488 donor and Alexa-546 acceptor dyes at the ends of the DNA. FRET measurements were carried out to determine the end-to-end distance in the DNA complexed to T7 RNAP using steady state and

† This research is supported by NIH Grant GM 51966 to S.S.P.

* To whom correspondence should be addressed. E-mail: patelss@umdnj.edu. Telephone: (732) 235-3372. Fax: (732) 235-4783.

[1] Abbreviations: 2-AP, 2-aminopurine; A488, succinimidyl ester of 5(6)-Alexa Fluor 488 carboxylic acid; A546, succinimidyl ester of 5(6)-Alexa Fluor 546 carboxylic acid; FRET, fluorescence resonance energy transfer; NT, nontemplate strand; RNAP, RNA-dependent polymerase; TAMRA, tetramethylrhodamine.

10.1021/bi0522910 CCC: $33.50
Published on Web 03/22/2006

time-resolved methods. Studies were carried out with both duplex and premelted bubble promoters; the latter mimics the open form of the DNA, and therefore, studies with the bubble promoter provide information about DNA conformation in the open complex. Using a combination of 2-AP fluorescence and FRET, we have calculated the degree of promoter DNA bending in the closed and open complexes. This allowed us to estimate the free energy involved in DNA bending and opening during the formation of the open complex by T7 RNAP. The study also served as a starting point for developing a solution-based real-time assay to measure the DNA conformational changes during transcription initiation (*42*).

MATERIALS AND METHODS

Enzyme, Oligodeoxynucleotides, and Dye Coupling. T7 RNAP was isolated to >95% purity and determined to be free from contaminating exonuclease activity. The T7 RNAP concentration was determined from its absorbency value at 280 nm in 8 M urea using a molar extinction coefficient of 1.4×10^5 M^{-1} cm^{-1} (*24*). T7 RNAP was stored at −80 °C [in 20 mM sodium phosphate (pH 7.7), 100 mM NaCl, 1 mM Na_3-EDTA, 1 mM dithiothreitol, and 50% (v/v) glycerol].

Oligodeoxynucleotides were custom synthesized (Integrated DNA Technologies, Coralville, IA) and PAGE purified before use. Aminohexyl linker (C6) was incorporated at the 5′-terminus during DNA synthesis and reacted with a succinimidyl ester of 5(6)-Alexa Fluor 488 carboxylic acid (Alexa-488 or A488) or 5(6)-Alexa Fluor 546 carboxylic acid (Alexa-546 or A546) (Invitrogen Molecular Probes, Portland, OR). The coupling reaction was performed by mixing the DNA strand with a 10-fold excess of the dye molecule in 200 mM sodium carbonate buffer (pH 8.0) and leaving the mixture standing in the dark overnight at room temperature. After the unreacted dye had been removed by gel filtration (Biogel P-6, Bio-Rad), the labeled strand was purified from the unlabeled strand on a 14 to 16% polyacrylamide gel containing 5 M urea. Concentrations of the labeled DNA strands and the labeling ratio (dye/DNA) were determined spectrophotometrically using extinction coefficients of 71 000 M^{-1} cm^{-1} at 490 nm for A488 and 103 000 M^{-1} cm^{-1} at 550 nm for A546. The dye absorbance at 260 nm was corrected: $A_{real} = A_{obs} - (A_{\lambda_{max}}CF)$. $A_{\lambda_{max}}$ is the peak absorbance value of the coupled dye, and CF is the correction factor (0.28 for A488 and 0.21 for A546). In this manner, we were able to confirm that each DNA strand contained only one dye molecule. Double-stranded DNA was made by mixing the appropriate complementary strands in an equimolar ratio (for the doubly dye-labeled DNA) or with a 5% excess of the unlabeled strand (for the singly dye-labeled DNA), heating to 70−80 °C for 5 min, and slowly cooling the sample to room temperature over 2 h.

Steady State Fluorescence Anisotropy. Fluorescence anisotropy was measured in an L-format scheme using a PTI QM-3 spectrofluorimeter (Photon Technology International) mounted with the Glen-Thomson calcite prism polarizers and a thermoelectrically controlled cell holder. The equilibrium titration was conducted at 20 °C in the reaction buffer [50 mM Tris-acetate, 50 mM Na-acetate, 10 mM Mg-$(acetate)_2$, and 2 mM dithiothreitol (pH 7.5)] with 0.05 mg/mL bovine serum albumin (BSA) and 0.01% Tween 20. After each addition of T7 RNAP, the reaction mixture was incubated for 4−6 min before fluorescence measurement. Vertically and horizontally polarized emission fluorescence intensities (F_{vv} and F_{vh}, respectively) of the DNA-labeled dye were measured with vertically polarized excitation. Fluorescence anisotropy, $r_{obs} = (F_{vv} - GF_{vh})/(F_{vv} + 2GF_{vh})$, was calculated with the determined grating correction factor G. The observed anisotropy (r_{obs}) is a function of the anisotropies of both the free DNA (r_f) and the DNA in the complex (r_b):

$$r_{obs} = r_b f_b + r_f(1 - f_b) \quad (1)$$

f_b is the fraction of the total DNA ($[D_t]$) in the T7 RNAP−DNA complex. The equilibrium dissociation constant (K_d) was determined from fitting the dependence of observed anisotropy versus total T7 RNAP, $[P_t]$, to eqs 1 and 2.

$$f_b = \frac{K_d + [P_t] + [D_t] - \sqrt{(K_d + [P_t] + [D_t])^2 - 4[P_t][D_t]}}{2[D_t]} \quad (2)$$

In a case where the fluorescence intensity of the DNA-labeled dye was quenched by a factor Q, $f_b = (r_{obs} - r_f)/[Q(r_b - r_{obs}) + (r_{obs} - r_f)]$.

Steady State FRET Measurement. FRET efficiency (E_{FRET}) was determined at 20 °C using the $(ratio)_A$ method that normalizes the fluorescence of the sensitized acceptor due to FRET to the fluorescence of the labeled acceptor without FRET (*25*). The sensitized acceptor fluorescence was determined by correcting the fluorescence of donor-only DNA in the spectral range of 500−630 nm with excitation at 490 nm (em^D_{exD}) and from the fluorescence of donor−acceptor doubly labeled DNA (em^{DA}_{exD}) in the same wavelength range. The integrated sensitized acceptor fluorescence due to FRET (570−630 nm) was compared to the integrated acceptor fluorescence upon direct excitation at 550 nm (em^{DA}_{exA}) to extract the value of $(ratio)_A$:

$$(ratio)_A = \frac{em^{DA}_{exD} - \alpha em^{D}_{exD}}{em^{DA}_{exA}} \quad (3)$$

where α is a normalization factor of donor fluorescence in the absence and presence of FRET. The FRET efficiency, E_{FRET}, depends linearly on the value of $(ratio)_A$:

$$(ratio)_A = E_{FRET} d^+ \frac{\epsilon^D_{exD}}{\epsilon^A_{exA}} + \frac{\epsilon^A_{exD}}{\epsilon^A_{exA}} \quad (4)$$

where d^+ is the labeling ratio with the donor dye and equal to 1 and ϵ^D_{exD}, ϵ^A_{exA}, and ϵ^A_{exD} are the extinction coefficients of the donor and acceptor at their respective excitation wavelengths of 490 (exD) and 550 nm (exA), respectively. The $\epsilon^A_{exD}/\epsilon^A_{exA}$ value of 0.097 and the $\epsilon^D_{exD}/\epsilon^A_{exA}$ value of 0.68 were used. In the equilibrium titration of constant dye-labeled DNA with increasing concentrations of T7 RNAP, the binding fraction of DNA is related to the measured energy transfer efficiency E according to

$$f_b = (E - E_0)/(E_b - E_0) \quad (5)$$

E_0 and E_b are the starting and ending values, respectively. To obtain the equilibrium dissociation constant, K_d, the dependence of observed FRET efficiency versus total T7 RNAP, $[P_t]$, was fit by the least-squares method to the quadratic equation (eq 2).

Fluorescence Lifetime Decay. The fluorescence lifetime decay was measured at 20 °C on a PTI LaserStrobe fluorescence lifetime spectrometer interfaced with a nitrogen-pumped dye laser (PTI model GL-302 pumped by GL-3300). The laser output at 490 nm (dye PLD481) was coupled through fiber optics to the sample compartment and focused on the sample in a thermoelectrically controlled cell holder. The start and stop delays of the acquisition were set by a DG535 digital delay generator (Stanford Instruments). The instrument response function was detected at 490 nm using a dilute suspension of a nondairy creamer. The fluorescence decay at 520 nm was collected in the logarithm time mode in 500 channels with five laser shots per time point. The final decay curve reflected an average of at least six consecutive acquisitions. Observed fluorescence decay functions, $S(t)$, were deconvolved using a PTI Felix32 program to yield the fluorescence intensity decay function, $F(t)$, which was then analyzed as the sum of exponential.

$$F(t) = \sum_{i=1}^{n} \alpha_i \exp(-t/\tau_i) \tag{6}$$

where α_i and τ_i are the amplitude and lifetime, respectively, of each component. Data analysis was executed with a nonlinear least-squares algorithm and iterative deconvolution. The goodness of fit was judged by visual inspection and by the value of the reduced error parameter, χ^2. The amplitude-weighted fluorescence lifetime of donor, $\langle\tau_D\rangle$, was calculated according to eq 7.

$$\langle\tau_D\rangle = (\sum_{i=1}^{n} \alpha_i\tau_i)/(\sum_{i=1}^{n} \alpha_i) \tag{7}$$

The weighted lifetimes of the donor in the absence and presence of acceptor, τ_D and τ_{DA}, respectively, were then used to calculate the FRET efficiencies, E_{FRET}, according to the following equation:

$$E_{FRET} = 1 - \tau_{DA}/\tau_D \tag{8}$$

End-to-End Distance Determination. The end-to-end distance of a linear DNA labeled with the donor−acceptor dye pair was calculated from a cylindrical model on the basis of the helical geometry of the B-type duplex DNA in aqueous solution (*25*). Experimentally, the end-to-end distance of a linear or curved duplex DNA can be determined using the donor- and acceptor-labeled DNA and by measuring the FRET efficiency:

$$R = R_o[(1 - E_{FRET})/E_{FRET}]^{1/6} \tag{9}$$

where R_o is the Förster radius at which 50% of E_{FRET} occurs and R is the actual D−A distance measured from E_{FRET}. Values of E_{FRET} determined from the steady state and time-resolved FRET methods were comparable. R_o was determined from eq 10.

$$R_o^6 = (8.785 \times 10^{-5})\phi_D\kappa^2 n^{-4} J(\upsilon)\ \text{Å}^6 \tag{10}$$

The refraction index, n, was assumed to be 1.33. ϕ_D is the quantum yield of the DNA-tethered donor dye in the absence of the acceptor dye. Using quinine sulfate in 0.1 M H_2SO_4 as the standard reference, ϕ_D of DNA-attached A488 was determined to be 0.84, which is smaller than the value of 0.97 determined for the free dye. The low anisotropy of labeled A488 and A546 in the protein complex suggests a random orientation of the donor−acceptor pair attached on DNA, which justifies $^2/_3$ as a good approximation of the relative orientation factor κ^2. The spectral overlap integral, $J(\upsilon)$, between the donor fluorescence spectrum and the acceptor absorbency spectrum was calculated from eq 11.

$$J(\upsilon) = \sum F_{D(\lambda)}\epsilon_{A(\lambda)}\lambda^4\, d\lambda / \sum F_D(\lambda)\, d\lambda\ M^{-1}\ cm^{-1}\ nm^4 \tag{11}$$

where $F_{D(\lambda)}$ represents the fluorescence intensity of the attached donor in the absence of FRET at wavelength λ and $\epsilon_{A(\lambda)}$ is the extinction coefficient of the tethered acceptor. The overlap integral $J(\upsilon)$ was determined to be 2.24×10^{15} by numerical integration with a 1 nm interval. The calculated Förster distances (R_0) of 61.4 Å for the donor−acceptor pair and 63.8 Å for the free dye pair in solution are in good agreement with the reference value of 64 Å (*26*).

Stopped-Flow FRET. Rapid assay of the effect of adding an initiating nucleotide analogue 3′-dGTP on the fluorescence intensity of doubly labeled DNA preincubated with T7 RNAP was performed at 25 °C on a KinTek SF-2003 stopped-flow setup (KinTek Corp., Austin, TX) equipped with computer-controlled motor-driven syringes. Equal volumes (20 μL) of preformed binary complex of 80 nM T7 RNAP and 40 nM dye-labeled DNA (duplex or bubble promoter) were mixed with 1 mM 3′-dGTP. The dead time of data acquisition in this system was 1−2 ms, and the fluorescence signals were measured in a T-format scheme on 1000 channels. A 520 nm band-pass filter was used to collect the donor A488 fluorescence emission without interference from the acceptor signal, while a 570 nm cutoff filter was used to collect the acceptor A546 fluorescence. Approximately 10−15 shots were collected and averaged to yield the time traces of donor and acceptor fluorescence. Measurements were conducted in standard reaction buffer without BSA and detergent Tween 20.

2-Aminopurine Fluorescence Changes. The distribution of closed and open complexes was determined through measurements of the fluorescence intensity of 2-AP incorporated at position −4 in the template strand upon binding to T7 RNAP (*13*, *16*). Experiments were carried out in a 3 mL quartz cuvette at 20 °C on a FluoroMax-2 spectrofluorometer (Jobin Yvon-Spex Instruments S.A., Inc.). Fluorescence intensities of 100 nM 2-AP incorporated duplex promoter or bubble promoter in the absence or presence of 200−800 nM T7 RNAP were collected from 350 to 420 nm (4 nm bandwidth) with excitation at 320 nm (2 nm bandwidth). The concentration of 2-AP DNA was normalized by UV absorbance measurements. After the contributions from buffer and protein had been subtracted, the corrected 2-AP fluorescence was integrated between 350 and 400 nm. Fluorescence measurements of duplex promoter in the

Table 1: Oligodeoxynucleotide Sequences[a]

DNA	Sequence
Duplex promoter	-22 +1 +9
	NT: 5′ TAAATTAATACGACTCACTATAGGGAGACTA
	T: 3′ ATTTAATTATGCTGAGTG**A**TATCCCTCTGAT
Bubble promoter	mutNT: 5′ TAAATTAATACGACTCAC<u>CCGCAT</u>GAGACTA
	T: 3′ ATTTAATTATGCTGAGTG**A**TATCCCTCTGAT

[a] The dyes Alexa-488 and Alexa-546 were covalently attached to the 5′-ends of the NT (or mutNT) and the T strand via a C6 linker to make dye-labeled strands A488−NT (or A488−mutNT) and A546−T, respectively. The bubble promoter contained multiple mutations from position −4 to +2 (underlined) on the nontemplate strand. The fluorescent base 2-AP was substituted for the adenine at position −4 (bold) in the T strands to make 2-AP-labeled promoters (2-AP−T).

presence of 0.5 mM 3′-dGTP were carried out in the same manner.

RESULTS

T7 RNAP-Induced FRET Changes in the Duplex Promoter DNA. Alexa-488 (donor) and Alexa-546 (acceptor) were covalently attached to the 5′-end of the nontemplate and template strands, respectively (Table 1). Absorbance measurements confirmed that the DNA strands were labeled with the dyes in a 1:1 ratio. The labeled template and nontemplate strands were annealed to create a 31 bp duplex promoter with the T7 ϕ10 promoter sequence and dyes at the opposite ends. This doubly dye-labeled promoter DNA was used to investigate T7 RNAP-induced conformational changes in the promoter DNA fragment. Figure 1A shows the steady state fluorescence spectra of the duplex promoter normalized on the donor side in experiments that contained (i) donor-only promoter, (ii) unliganded donor−acceptor doubly dye-labeled promoter, and (iii) T7 RNAP-bound doubly dye-labeled promoter. These experiments showed that in the presence of T7 RNAP, the fluorescence intensity of the acceptor A546 attached to the duplex promoter increased (sensitized acceptor) relative to the free DNA. This result was confirmed further by measuring similar fluorescence changes in experiments where the dye positions were interchanged on the duplex promoter or by using a different donor−acceptor pair such as tetramethylrhodamine−Alexa-647 (data not shown). Control experiments showed that the fluorescence intensity of the singly dye-labeled promoter remained unchanged upon addition of T7 RNAP. The results indicate that the observed fluorescence changes in the donor- and acceptor-labeled promoter upon T7 RNAP addition are due to energy transfer rather than due to protein−dye interactions. The observed increase in FRET efficiency indicates a shortening of the end-to-end distance in the dye-labeled promoter DNA when it is complexed to T7 RNAP.

To determine the maximal T7 RNAP-induced energy transfer efficiency, doubly and singly dye-labeled duplex promoters were titrated with increasing concentrations of T7 RNAP and the FRET efficiency was calculated from the sensitized acceptor fluorescence using the steady state $(\text{ratio})_A$ method as detailed in Materials and Methods. In the absence of T7 RNAP, the FRET efficiency of the duplex promoter was 0.02 and it increased to a maximum value of 0.05−0.06 at saturating concentrations of T7 RNAP (Figure 1B). Fluorescence anisotropy changes were measured simultaneously by selectively exciting the acceptor at 550 nm and measuring its polarized emission signal at 580 nm. Both FRET and anisotropy changes followed the same binding process under equilibrium conditions (Figure 1B). Using the least-squares method, the anisotropy and FRET binding data were fit to the quadratic equation (eqs 1 and 2 and eqs 5 and 2, respectively) to obtain a T7 RNAP−DNA K_d of 1−2 nM, which is in good agreement with the K_d of 4 nM determined previously for longer promoter constructs (40 bp) with the upstream end at position −22 (*27*, *28*). Multiple titrations were performed to reduce the error in the observed FRET efficiency, and the mean E_{FRET} is summarized in Table 2.

The efficiency of energy transfer obtained from the steady state $(\text{ratio})_A$ method was further confirmed by measuring the fluorescence lifetime decay of the donor-labeled promoter DNA both in the absence and in the presence of acceptor as outlined in Materials and Methods. Figure 2 shows the fluorescence lifetime decay of A488 in the doubly dye-labeled DNA with and without T7 RNAP. The donor fluorescence lifetime decay was fit to two populations as judged by the random distribution of residuals (small panels in Figure 2) and the χ^2 values (Table S1 of the Supporting

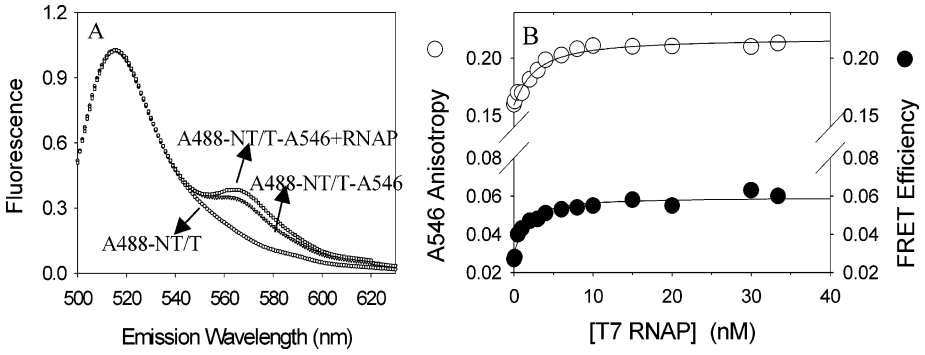

FIGURE 1: T7 RNAP-induced FRET and anisotropy changes. (A) Steady state fluorescence emission spectra (normalized to donor fluorescence) of the 31 bp A488- and A546-labeled duplex promoter (10 nM) in the absence (▽) and presence (□) of 100 nM T7 RNAP at 20 °C. The emission spectrum of unliganded A488-labeled duplex DNA (A488−NT/T) is shown for comparison (○). The samples were excited at 490 nm, and emission was scanned from 500 to 630 nm. Induced FRET upon T7 RNAP binding is demonstrated by the sensitized acceptor fluorescence peak at ~575 nm. (B) The fluorescence anisotropy of A546 (○) and FRET efficiency (●) of the duplex promoter (2 nM) were measured with increasing T7 RNAP concentrations. Anisotropy was measured by selectively exciting the A546 label in the duplex promoter at 550 nm and by monitoring perpendicular and parallel intensities at 585 nm. FRET efficiency was calculated from the sensitized acceptor fluorescence using the $(\text{ratio})_A$ method (Materials and Methods).

Table 2: End-to-End Distances and DNA Bending Angles of T7 Promoter Fragments[a]

sample	FRET efficiency (%) (ratio)$_A$	FRET efficiency (%) lifetime	R (Å)[b]	bend angle[c] (deg)
A488NT/A546T	2.2 ± 2.2	2.5 ± 1.4	(113 ± 8)	
A488NT/A546T + T7RNAP	5.5 ± 3.2	6.3 ± 1.9	99 ± 7 [d]	~50[d]
A488NT/A546T + 3′-dGTP + T7 RNAP	10.1 ± 1.8	11.7 ± 1.4	88 ± 2	79 ± 5
A488NTmut6/A546T	1.5 ± 1.3	3.4 ± 1.3	(112 ± 6)	
A488NTmut6/A546T + T7 RNAP	11.0 ± 1.1	13.0 ± 0.9	86 ± 2	86 ± 5

[a] The FRET efficiency of Alexa-488 and Alexa-546 dyes labeled at either end of the promoter DNAs was determined from the (ratio)$_A$ approach (eqs 3 and 4) and from the fluorescence lifetime decay of the donor (eq 8). [b] The end-to-end distances of the promoter DNAs were determined from the averaged FRET efficiency values obtained using both the steady state and lifetime decay approaches. Results in parentheses were calculated from <5% FRET efficiency and thus are less accurate. [c] The bending angle was calculated assuming a single-kink model with the bending center at position −1 on the promoter. [d] As the FRET values are weighted averages for the closed and open complexes, both the D−A distances and bend angle shown here were also averaged values for the two complex forms (see the text).

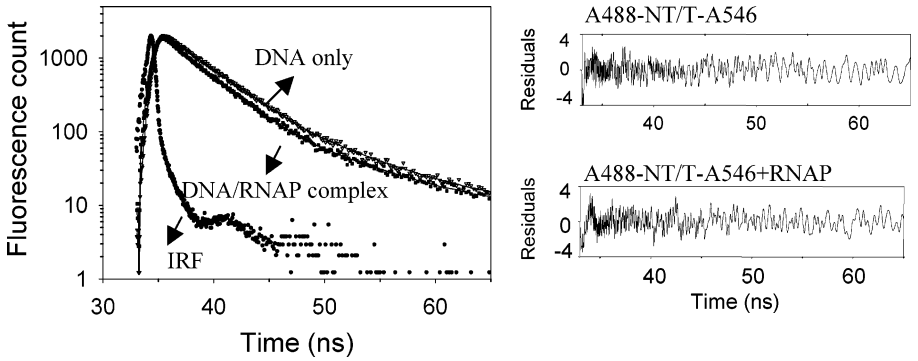

FIGURE 2: Fluorescence lifetime decay of the dye-labeled duplex promoter. The time-resolved fluorescence decay was collected at 520 nm with excitation at 480 nm. The decay curves of A488- and A546-labeled duplex promoter (40 nM) in the absence and presence of 200 nM T7 RNAP are shown with the instrumental response function (IRF) curve. Smooth and continuous curves represent ideal fits to a biexponential equation (residuals are shown in the adjacent small panels).

Information). The average excited lifetime of the donor attached to the duplex promoter (calculated from eq 7) becomes slightly shorter in the presence of T7 RNAP, which was used to calculate the energy transfer efficiency (eq 8). Table S1 shows the fitted parameters for the donor fluorescence lifetime decay experiments, and Table 2 shows the FRET efficiency values calculated from multiple measurements. Steady state and fluorescence lifetime decay experiments provided consistent values of low-energy transfer efficiency for the duplex promoter. From the FRET values, an end-to-end distance of ~113 Å was calculated (eq 9) for the free duplex promoter DNA. This calculated distance is very close to the value of 115 Å obtained using a model that assumes a cylindrical DNA structure in aqueous solution with a B-type helical geometry (Figure 6 legend) (*25*, *29*). The slight increase in FRET in the presence of T7 RNAP indicates a slightly shortened end-to-end distance of 99 Å of the duplex promoter DNA complexed with T7 RNAP.

T7 RNAP-Induced FRET Changes in the Premelted Bubble Promoter. Several studies have indicated that the initiation complex of T7 RNAP in the absence of the initiating nucleotides contains a mixture of closed and open complexes that are in equilibrium that favors the formation of the closed complex (*12*−*14*). In the absence of the initiating nucleotides, therefore, both open and closed complexes contribute to the observed FRET value. To tease out the contribution of the open complex to the FRET value, we used a premelted 31 bp promoter fragment (bubble promoter) that has contiguous mismatches from position −4 to 2 (Table 1). Such a premelted DNA promoter has been shown to be transcriptionally active and to mimic the open complex conformation (*30*−*32*). The dyes A488 and A546 were attached to the opposite ends of the bubble promoter. Figure 3A shows the normalized fluorescence emission spectra of the A488- and A546-labeled bubble promoter (A488−mutNT/T−A546) with and without T7 RNAP. The sensitized acceptor intensity increased to a greater extent in the bubble promoter complex than in the duplex promoter complex.

The bubble promoter was titrated with increasing concentrations of T7 RNAP, and the steady state FRET and A546 anisotropy changes were measured (Figure 3B). The energy transfer value of the free bubble promoter is similar to that of the duplex promoter (<0.02), which indicates that the multiple mismatches do not change the end-to-end distances in the unliganded DNA, which has been observed previously (*33*). At saturating concentrations of T7 RNAP, the FRET efficiency of the bubble promoter increased to 0.12. Similar results of FRET changes were obtained from the fluorescence lifetime decay of A488 attached to the bubble promoter (Table 1S). The larger FRET change indicates a shorter end-to-end distance of the bubble DNA (86 Å) relative to that of the duplex DNA in their respective binary complexes. Both FRET and anisotropy titration curves in Figure 3B indicate that the titrations were performed under stoichiometric conditions. This is consistent with the K_d of ~5 pM of this six-mismatch bubble DNA (*42*).

DNA FRET Changes in the Pretranscribing Open Complex. Initiating nucleotides have been shown to stabilize the open complex of T7 RNAP and hence drive the initiation reaction to complete formation of the open complex (*13*, *14*, *16*). The effect of the initiating nucleotide analogue (3′-dGTP) on FRET efficiency changes was examined with the

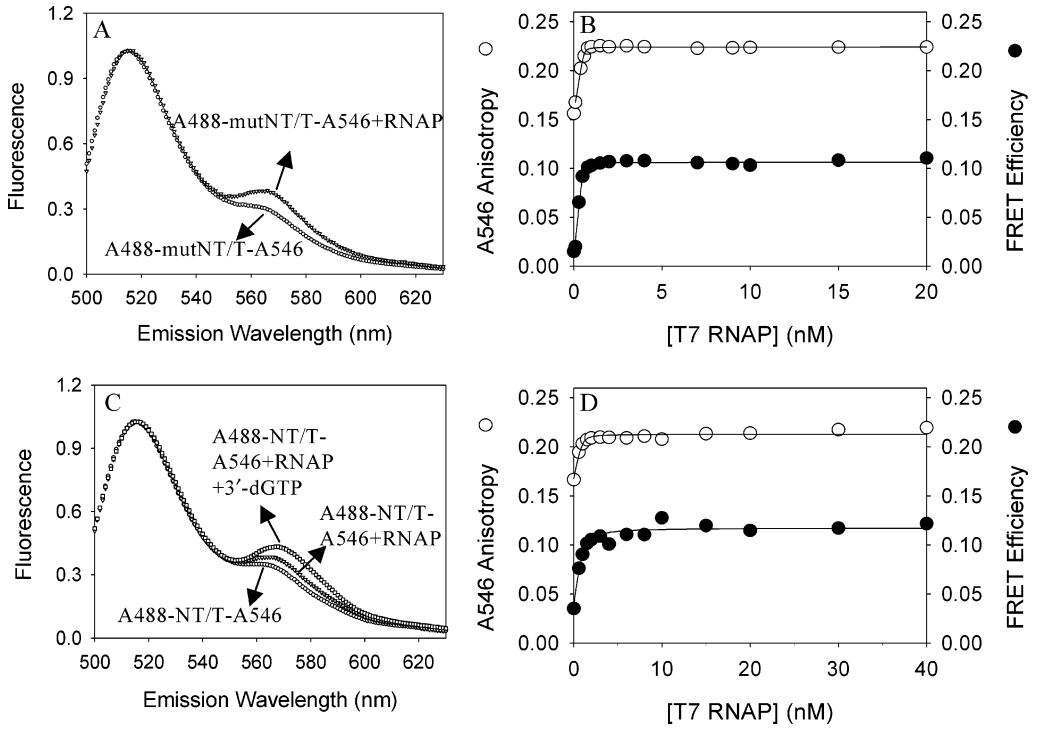

FIGURE 3: T7 RNAP-induced FRET and anisotropy changes in the bubble promoter and effect of the initiating nucleotide on the values of the duplex promoter. (A) Normalized steady state fluorescence emission spectra of the doubly dye-labeled bubble promoter (10 nM) in the absence (○) and presence (▽) of 100 nM T7 RNAP at 20 °C. (B) The fluorescence anisotropy of the A546 attached to the bubble promoter (1 nM) (○) and the FRET efficiency between the dye pair (●) attached to the bubble promoter depend on T7 RNAP concentration. **(**C**)** Normalized steady state fluorescence emission spectra of the doubly dye-labeled duplex promoter (10 nM) in the absence (○) and presence (□) of 100 nM T7 RNAP and 0.5 mM 3′-dGTP at 20 °C. (D) The dye-labeled duplex promoter (1 nM) was titrated with increasing T7 RNAP concentrations in the presence of 0.5 mM 3′-dGTP, and the fluorescence anisotropy (○) of tethered A546 and the FRET efficiency (●) were measured. The titrations reflected by FRET and anisotropy changes in both panels B and D were performed under stoichiometric conditions.

duplex promoter. Figure 3C shows the normalized fluorescence emission spectra of A488−NT/T−A546 fully complexed to T7 RNAP with and without 0.5 mM 3′-dGTP. The enhancement of acceptor fluorescence intensity in the ternary complex with the initiating nucleotide relative to the binary complex is clearly seen. Figure 3D also shows the A546 anisotropy and FRET efficiency changes in the duplex promoter upon titration with increasing concentrations of T7 RNAP in the presence of 3′-dGTP. The T7 RNAP complex with the duplex promoter is stabilized by the presence of 3′-dGTP as both FRET and anisotropy titration curves in Figure 4D are shifted to lower protein concentrations relative to those curves shown in Figure 1B. The $(\text{ratio})_A$ method and the donor fluorescence lifetime decay values provided a higher FRET value of 0.11 for the duplex promoter in the ternary complex with 3′-dGTP. This FRET value is nearly twice that of the duplex promoter complex in the absence of the nucleotide and similar to that of the binary complex of the bubble promoter. Thus, the duplex promoter in the ternary pretranscription complex and the bubble promoter in the binary complex assume the same global conformation in terms of DNA end-to-end distance, and this is significantly different from the conformation that the duplex promoter assumes in the absence of initiating nucleotides.

3′-GTP-Induced FRET Changes in the Duplex and Bubble Promoters. Stopped-flow FRET measurements were performed to investigate 3′-dGTP-induced DNA conformational changes in the binary complexes of the duplex and the bubble promoters. A mixture of 40 nM A488- and A546-labeled promoter (duplex or bubble) and 80 nM T7 RNAP was incubated in one syringe, and 1 mM 3′-dGTP was added from a separate syringe of the stopped-flow apparatus. A 520 nm band-pass filter was used to selectively monitor donor fluorescence from 515 to 525 nm without significant interference from A546, and a second 570 nm cutoff filter was used to monitor acceptor fluorescence. When the binary complex of the duplex promoter was mixed with a solution of 3′-dGTP, the donor fluorescence decreased and the acceptor fluorescence increased, indicating an enhancement of FRET (Figure 4A). In contrast, the binary complex of the bubble promoter when mixed with 3′-dGTP showed no observable fluorescence changes due to FRET (Figure 4B). These results support the idea that minimal changes occur in the promoter conformation during the transition from the binary open complex to the ternary pretranscription complex.

Coupled Changes in 2-AP Fluorescence and FRET. In the absence of initiating nucleotides, the formation of both closed and open complexes contributes to the values of FRET changes. To estimate the DNA conformation in the closed complex, we need to determine the contribution of the closed complex to the measured FRET values. The distribution of the closed to open complexes with the 31 bp promoter used in this study was determined using the same 2-AP fluorescence method that was used previously (*12*, *13*, *16*). The fluorescent adenine base analogue 2-AP was introduced in place of the adenine at position −4 in the template strand in the duplex and bubble promoters. Unstacking of the 2-AP base in the open complex results in a large increase in the fluorescence of 2-AP. The results summarized in Figure 5 show that the 2-AP fluorescence is lower in the binary

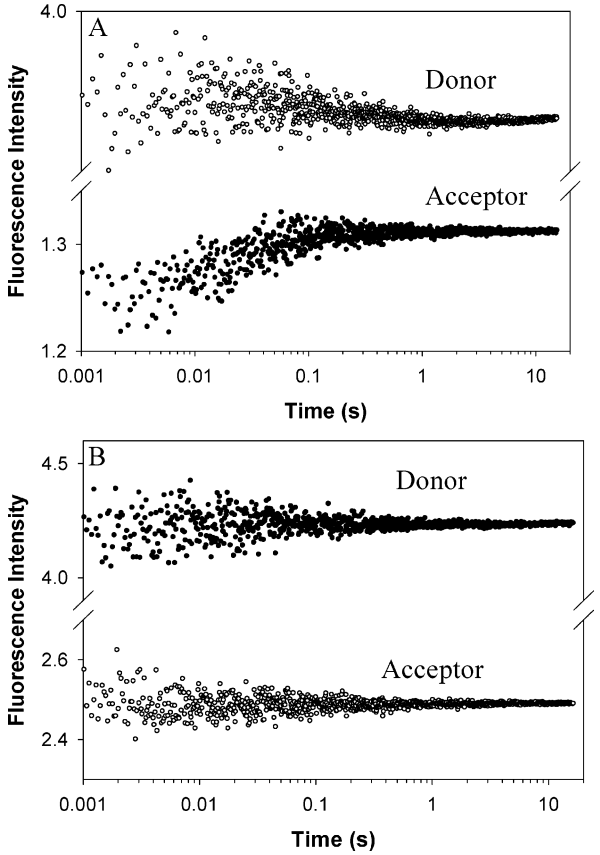

FIGURE 4: Stopped-flow kinetics of FRET changes induced by initiating nucleotide binding. A488- and A546-labeled duplex promoter (40 nM) was preincubated with T7 RNAP (80 nM), and the complex was rapidly mixed with 1 mM 3′-dGTP at 25 °C (final concentrations in parentheses). After excitation at 490 nm, the emission intensity was measured using a band-pass filter at 520 ± 5 nm for the donor A488 (top trace) and a cutoff filter at 570 ± 5 nm for the acceptor (bottom trace). More than 10 traces were collected and averaged to improve the signal-to-noise ratio. (B) The same experiment under the same conditions was carried out with the doubly dye-labeled bubble promoter.

complex of the duplex promoter than in the bubble promoter complex. Figure 5 also shows the same trend in the corresponding FRET values of the duplex and bubble promoters. These results indicate that local (opening) and global (end-to-end distance) DNA deformations are smaller in the duplex promoter than in the bubble promoter complex. When 3′-dGTP was added to the duplex promoter complex, the 2-AP fluorescence increased and the value became close to that of the bubble promoter complex. With the assumption that the DNA base pairs are not disrupted in the closed complex and the bubble DNA forms 100% open complex, we estimate that only 20% of the complexes with the duplex promoter are open complexes in the absence of the initiating nucleotides.

DISCUSSION

The FRET studies in this paper show that the end-to-end distance in the T7 promoter DNA fragments shortens when the promoters bind to T7 RNAP in the initiation complex. Recent studies have indicated that a minimal promoter for tight T7 RNAP binding requires a consensus sequence from base pair −22 to −5 (*27*, *28*). Therefore, we constructed our DNA fragments from base pair −22 to 9 to carry out FRET measurements in a stable complex with T7 RNAP. The FRET efficiency of the duplex promoter increased only slightly relative to that of free DNA when it formed a complex with T7 RNAP. On the other hand, the same size premelted promoter (a six-mismatch bubble promoter) showed a significant increase in FRET efficiency when it formed a complex with T7 RNAP. The presence of six mismatches in the bubble promoter alone does not contribute to the enhancement of FRET efficiency. When initiating nucleotides were added, the FRET efficiency of the duplex promoter complex increased to the extent observed for the bubble promoter complex, whereas no such increase was seen for the bubble promoter complex. The observed increase in FRET efficiency was attributed to a shortening of the end-to-end distance in the dye-labeled DNA (R_{D-A}) by T7 RNAP. On the basis of these FRET measurements, R_{D-A} values were calculated according to eq 9 and summarized in Table 2. As expected, free duplex promoter and bubble promoter had similar R_{D-A} values. When the promoter was complexed to T7 RNAP, but in the absence of 3′-dGTP, the R_{D-A} of the duplex promoter was longer than that of the bubble promoter. The R_{D-A} of the duplex promoter in the presence of 3′-dGTP was shortened and nearly the same as that of the bubble promoter in the binary complex. If we assume that T7 RNAP forms a homogeneous binary complex with each of these promoter fragments, then these results indicate that duplex and bubble promoters generate different types of complexes with T7 RNAP.

Previous initiation kinetics studies have indicated that T7 RNAP does not form a homogeneous binary complex with the duplex promoter (*12*−*14*, *16*). The initial binding of T7 RNAP to the duplex promoter results in a mixture of closed and open complexes. The equilibrium of this reaction favors the closed conformation, unless initiating nucleotides are present to stabilize the open complex (*13*, *14*, *16*). A similar observation was also made for the stabilization of an *E. coli* open complex at the ribosomal RNA promoters by initiating nucleotides (*34*). Studies of permanganate reactivity sensitive to single-stranded thymines in the DNA also support an unopened state of the TATA region in a linear duplex promoter in the binary complex and an open state in the presence of the initiating nucleotides or when supercoiled DNA is used (*35*−*37*). To make a homogeneous open complex in the absence of the initiating nucleotides, partially duplex (pds DNA) or bubble promoters (four to eight mismatched base pairs in the TATA region) are used. Kinetic studies have shown that the bubble promoter or the partially duplex promoter forms an open binary complex without the accumulation of a stable closed complex intermediate (*13*, *16*). The disruption of base pairing in the TATA region in these premelted promoters strongly disfavors the closing of the initial bubble and therefore stabilizes the open complex. Equilibrium measurements demonstrate that the premelted promoter binds to T7 RNAP with a nearly 1000-fold higher affinity than the duplex promoter (*32*), indicating that T7 RNAP makes optimal interactions with the premelted promoter.

The observed differences in the R_{D-A} values for the duplex and bubble promoter binary complexes can be explained by the presence of both open and closed complexes in the duplex promoter reaction and by the promoter DNA being bent to different extents in the closed and open complexes of T7

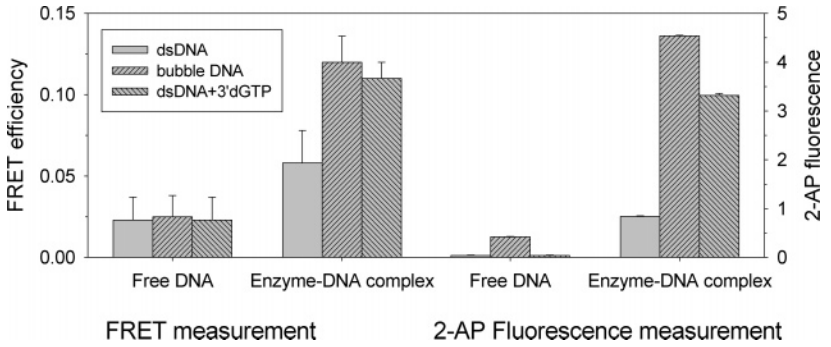

FIGURE 5: FRET and 2-AP fluorescence of various T7 RNAP−promoter complexes. The two left-most groups of bar graphs show the FRET efficiency values for the duplex and bubble promoters in the absence and presence of T7 RNAP (Table 2) and the duplex promoter in the presence of 0.5 mM 3′-dGTP, respectively. The two right-most groups of bar graphs show the relative 2-AP fluorescence intensities of 100 nM duplex and bubble promoters in the absence and presence of a saturating concentration of T7 RNAP (400−800 nM) and the duplex promoter in the presence of 0.5 mM 3′-dGTP, respectively.

RNAP. Determination of the bending angle from the relationship between the end-to-end distances of the unbent DNA (R_f) and bent DNA (R_b) is model-dependent. Here we use a single-kink model to calculate the DNA bending angle (α) based on the relationship $R_b^2 = L_1^2 + L_2^2 + 2L_1L_2 \cos \alpha$ (Figure 6). The DNA lengths upstream and downstream of the bending center, L_1 and L_2, respectively, can be determined from the position of the bending center and the overall end-to-end length ($R_f = L_1 + L_2$) of the free DNA. In the free DNA, the upstream-labeled A488 and the downstream-labeled A546 are on the opposite faces of the helix. Modeling indicated that the downstream template strand is untwisted by ~146° in the initiation open complex with a three-nucleotide RNA (*3*). This changes the relative orientation of the dyes from opposite faces in the free DNA to nearly the same face in the open complex, which contributes to a shortening of the distance between the dyes. To correct for the shortening in the DNA end-to-end distance due to untwisting in the open complex, we assumed that the free DNA was untwisted similarly as in the open complex. This provided a corrected R_f* value of 110 Å that was used to compare to the measured D−A distances in the open complexes.

From the FRET efficiency values, an end-to-end distance of ~86 Å was calculated for the bubble promoter bound to T7 RNAP (Table 2), which is significantly shorter than that of the free DNA. A similarly shortened D−A distance was calculated for the duplex promoter in the 3′-dGTP-stabilized complex. Applying the geometric model of DNA bending described above and assuming the bending center at position −1 (*1*) and unwinding of the downstream DNA, we calculated a bend angle of 86 ± 5° for the bubble promoter complex and 79 ± 5° for the duplex promoter in the 3′-dGTP-stabilized complex. Thus, the duplex promoter and bubble promoter are bent to equivalent extents in their open complexes. If the bending center was at position −4 rather than position −1, the calculated bend values will decrease by <5°. Similarly, without the DNA untwisting correction, the calculated DNA bend angles would be ~10° higher. Overall, these results indicate that the promoter DNA is sharply bent in the preinitiation open complex.

Although the closed form of the promoter DNA complexed to T7 RNAP is suggested by biochemical and fluorescence data, little is known about its structure and interactions with T7 RNAP. The crystal structure of T7 RNAP in complex with a 17 bp promoter with the downstream template DNA completely melted and bound in the cleft of the RNAP is likely that of the open complex (*17*). Using a combination of 2-AP fluorescence changes and FRET efficiency changes, we have estimated a 20:80 distribution of the open and closed

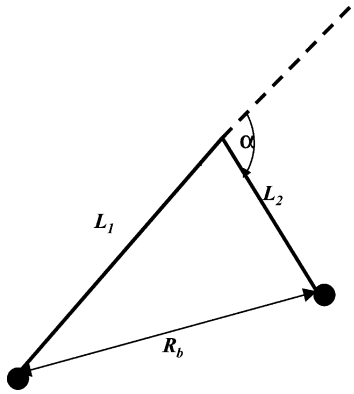

FIGURE 6: Geometrical model for the bent DNA in the T7 RNAP complex. The end-to-end distance (R_f) of an ideal linear DNA doubly labeled with a D−A pair was calculated from a cylindrical model for the B-type duplex DNA in aqueous solution (typically 20 Å diameter, 3.4 Å rise, and 360° per full turn) according to the relation $R_f = \sqrt{(3.4N+L_{LK})^2+[L_D^2+L_A^2-2L_DL_A\cos(36N+\phi)^2]}$, where N is the number of base pairs between the attached donor and acceptor dyes ($N = 30$) in the duplex DNA, L_{Lk} is the D−A distance without interruption from the duplex DNA base pairs and estimated to be 6 Å for a fully stretched C6 amino linker, L_D and L_A are the normal distances from the donor and acceptor dyes, respectively, to the helical axis, and ϕ is a constant interdye angle without base pair separation participating in the angular separation that includes that of dye-attached phosphates. The values of L_D, L_A, and ϕ were not experimentally determined for the D−A pair used here. On the basis of the similar labeling chemistry and fluorescence anisotropy of the well-studied D−A pair (fluorescein and tetramethyrhodamine) (*25*), the following values were used: $L_D = 25$ Å, $L_A = 15$ Å, and $\phi = 220°$. Using this ideal linear DNA model, the end-to-end distance of the doubly labeled 31 bp duplex promoter was calculated as 115 Å, which is close to that estimated from the energy transfer measurements. The end-to-end distance (R_b) of the bent DNA in the complex of T7 RNAP was determined from FRET efficiency measurements. A noncentered single-kink model was used to calculate the DNA bend angle, α. The bending center was assumed to be at position −1 and flanked by 21 bp (L_1) and 9 bp (L_2) DNA. The bending angle α was calculated from $\cos(\alpha) = (R_b^2 - L_1^2 - L_2^2)/2L_1L_2$. To correct the effect of strand untwisting (φ in degrees) in the initiation open complex (see the text), the angular separation in the equation was revised to be $36N + \phi + \varphi$ correspondingly. In this case, values of 77 and 33 Å were set for L_1 and L_2, respectively.

complexes in the T7 RNAP initiation reaction with the duplex promoter. Knowing the FRET value of the DNA in the open complex from studies of the bubble promoter, we estimated after subtracting the 20% contribution of the open complex to the observed FRET that the closed complex FRET efficiency is ~0.02. Given that the unliganded T7 promoter has an intrinsic bend of ~15° as indicated by our FRET studies and previous gel electrophoresis studies (*1*), we estimated that the DNA bend induced by T7 RNAP is ≤25° in the closed complex, which is significantly smaller than the DNA bend in the open complex. Without correction of the FRET contribution from the open complex, however, the calculation based on the observed ~0.05 FRET efficiency for the duplex promoter complex will lead to an estimated DNA bend angle of ~50°, which would be consistent with a previous result obtained through the analysis of gel electrophoresis anomalies for the duplex promoter without initiating nucleotides (*1*). Thus, DNA bending of ~86° measured for the bubble promoter complex would represent the actual bending of the promoter DNA in the open complex. The apparent DNA bend angles of ~50° calculated here and 40−60° from the gel electrophoresis anomalies (*1*) for the duplex promoter complex represent an *average* angle with contributions from both the closed and open complexes. This idea is supported by the result that the observed DNA bend angles in the duplex and bubble promoters were nearly the same in the presence of 3′-dGTP, conditions under which the initiation complex is as predominant as the open complex. Therefore, T7 RNAP-induced DNA bending is most significant in the open complex, and the bend angle for the pretranscribing open complex from our FRET studies is close to that obtained from structure modeling of the early initiation complex (*3*).

From the DNA bending angles in the closed and open complexes, we are able to calculate the free energies associated with DNA bending (ΔG_{bend}) according to the wormlike chain model $\Delta G_{bend} = RTP\alpha^2/2L$, where R is the gas constant, T is the temperature in kelvin, L is the contour length of the DNA bent by angle α in radians, and the persistence length of the DNA P is ≈150 bp or 50 nm (*38*). In the T7 RNAP−promoter open complex, the upstream and downstream DNA axes lose the continuity of their relative orientation within the region from position −4 to 2 (*3*). For the closed complex, however, there is no structural information about the DNA conformation. Using 25° as the upper limit of the RNAP-induced DNA bend angle in the closed complex and assuming 6 bp in the bend, a ΔG_{bend1} to form the closed complex is calculated as 1.4 kcal/mol at 20 °C. The ΔG_{bend1} would be 2−3 times larger if the bend were confined to a smaller region, and this energy would be smaller if the bend were distributed over a larger region. From the bend angle in the open complex, ΔG_{bend2} is calculated to be 4.7 kcal/mol. Thus, the roughly estimated total energy cost, ΔG_{bend}, for T7 RNAP-induced DNA bending is 6.1 kcal/mol.

A simplified energetic sketch of the events that occur during promoter DNA binding and opening is shown in Figure 7. The intrinsic free energy of duplex promoter binding, ΔG_{bind}, has not been measured experimentally but can be deduced from the experimentally observed ΔG_{ds} as follows. ΔG_{ds} is the net energy for the duplex promoter−T7 RNAP complex after the cost of duplex DNA deformations has been subtracted. The experimentally observed ΔG_{ds} can be calculated from the K_d value (2 nM) of the T7 RNAP−duplex promoter complex and is equal to −11.7 kcal/mol. The open complex ($EP_{b/o}$, b/o represents the DNA bent and open in the open complex) is less stabilized by 0.8 kcal/mol relative to the closed complex ($\Delta\Delta G_{open} = \Delta G_{EP_{b/o}} - \Delta G_{EP_c}$) as estimated from the distribution of the two complexes (20% open and 80% closed) ($K_{eq} = [EP_{b/o}]/[EP_c] = 0.25$). Therefore, $\Delta\Delta G_{open} = 0.8$ and $\Delta G_{ds} = 11.7$ kcal/mol $= \Delta G_{bind} + \Delta G_{bend1} + 0.2\Delta\Delta G_{open}$. In this manner, we estimate that ΔG_{bind} equals −13.3 kcal/mol. The total penalty for DNA bending is 6.1 kcal/mol; therefore, the free energy of the hypothetically sharply bent DNA intermediate (EP_b), ΔG_{EP_b}, is −7.2 kcal/mol. EP_b is therefore much destabilized compared to the final $EP_{b/o}$ open complex ($\Delta G_{EP_{b/o}} = -11.1$ kcal/mol). Thus, additional energy is gained when the melted DNA strands in $EP_{b/o}$ interact with T7 RNAP. These simplified calculations indicate that a significant part of the promoter binding energy is invested in DNA bending and base pair melting occurs spontaneously upon DNA bending.

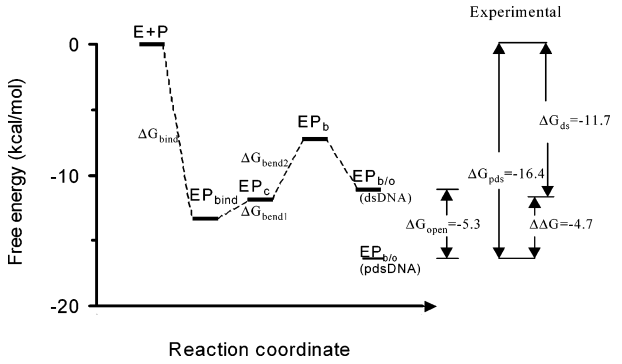

FIGURE 7: Energetics of bending and promoter DNA opening. The proposed thermodynamic dissection of free energies into steps of bending and opening. The free energy of binding of T7 RNAP to duplex DNA, ΔG_{bind}, is calculated as −13.3 kcal/mol, of which 1.4 kcal/mol (ΔG_{bend1}) is consumed on slightly bending the duplex DNA to form the closed complex (EP_c) and 4.7 kcal/mol (ΔG_{bend2}) on sharply bending the DNA to form the hypothetical intermediate, EP_b. Since the free energy difference between the open complex ($EP_{b/o}$) and the closed complex (EP_c) is only 0.8 kcal/mol ($\Delta G_{EP_{b/o}} - \Delta G_c = 0.8$ kcal/mol), open complex formation from EP_b is a spontaneous event. The net energy required for promoter opening is calculated from the difference in the energies of the premelted DNA complex and the opened and bent DNA complex: $\Delta G_{pds} - \Delta G_{EP_{b/o}} = -5.3$ kcal/mol, where pds represents a partially double-stranded DNA with the deletion of downstream NT strand from position −4, and ΔG_{pds} was calculated from its K_d of 1 pM for T7 RNAP (*32*).

A group of architectural proteins such as the TATA-binding protein (TBP), the lymphocyte enhancer factor-1 (LEF-1), and high-mobility group proteins (HMG) use minor groove intercalation of hydrophobic amino acid residues with contiguous base pair steps to induce DNA bending (*39*). These architectural proteins bend DNA with remarkably large angles in addition to untwisting the DNA strands and unstacking consecutive base pairs, thereby inducing opening of the downstream DNA. T7 RNAP may use a similar mechanism and use DNA bending energy to catalyze the formation of open complex. A part of the mechanism of open complex formation in T7 RNAP could involve the insertion of Val237 located at the tip of the intercalating β-hairpin into the minor groove of the promoter DNA near the TATA region (*3*, *17*, *18*). Mutational and partial deletion studies of

the intercalating β-hairpin indicate that the β-hairpin stabilizes the open complex but does not affect the kinetics of closed complex formation (*36*, *40*).

Structural and biochemical data suggest that T7 RNAP-induced bending of the promoter DNA is not limited to initiation. Structural and modeling studies suggest that the DNA is bent during the processive elongation phase of transcription by ~40° (*3*). FRET results suggest that promoter DNA bends similarly in the preinitiation complex and in the early initiation complex at least up to the abortive synthesis of three-nucleotide RNA (*3*), indicating no large structural changes in T7 RNAP during these steps (*17*, *18*). An approximate pathway of DNA bending from the unliganded promoter to the stable elongation can be described as follows: <15° (intrinsic bend in the promoter DNA) → <40° (closed complex) → ~83−86° (open complex) → ~80° (early initiation complex) → unknown structure (late initiation complex) → ~40° (stable elongation complex) with the bending center shifted to the downstream end. It is also known that the size and the position of the transcription bubble change during the transition from the initiation phase to the elongation phase (*41*). Different angles of DNA bending indicate changes in the protein−DNA contacts during the transition. Concomitant rearrangements of the protein structure are also known to occur in T7 RNAP (*2*, *3*). Thus, it will be useful to exploit the real-time FRET assay to probe the dynamic changes in the DNA conformation during transcription to gain more information about the intermediate complexes during the transition from initiation to elongation.

SUPPORTING INFORMATION AVAILABLE

One additional table of time-resolved fluorescence lifetime decay parameters. This material is available free of charge via the Internet at http://pubs.acs.org.

REFERENCES

1. Ujvari, A., and Martin, C. T. (2000) Evidence for DNA bending at the T7 RNA polymerase promoter, *J. Mol. Biol. 295*, 1173−1184.
2. Tahirov, T. H., Temiakov, D., Anikin, M., Patlan, V., McAllister, W. T., Vassylyev, D. G., and Yokoyama, S. (2002) Structure of a T7 RNA polymerase elongation complex at 2.9 Å resolution, *Nature 420*, 43−50.
3. Yin, Y. W., and Steitz, T. A. (2002) Structural basis for the transition from initiation to elongation transcription in T7 RNA polymerase, *Science 298*, 1387−1395.
4. Meyer-Almes, F. J., Heumann, H., and Porschke, D. (1994) The structure of the RNA polymerase-promoter complex. DNA-bending-angle by quantitative electrooptics, *J. Mol. Biol. 236*, 1−6.
5. Rees, W. A., Keller, R. W., Vesenka, J. P., Yang, G., and Bustamante, C. (1993) Evidence of DNA bending in transcription complexes imaged by scanning force microscopy, *Science 260*, 1646−1649.
6. Schinkel, A. H., Groot Koerkamp, M. J., Teunissen, A. W., and Tabak, H. F. (1988) RNA polymerase induces DNA bending at yeast mitochondrial promoters, *Nucleic Acids Res. 16*, 9147−9163.
7. ten Heggeler, B., and Wahli, W. (1985) Visualization of RNA polymerase II ternary transcription complexes formed in vitro on a *Xenopus laevis* vitellogenin gene, *EMBO J. 4*, 2269−2273.
8. Coulombe, B. (1999) DNA wrapping in transcription initiation by RNA polymerase II, *Biochem. Cell Biol. 77*, 257−264.
9. Heumann, H., Ricchetti, M., and Werel, W. (1988) DNA-dependent RNA polymerase of *Escherichia coli* induces bending or an increased flexibility of DNA by specific complex formation, *EMBO J. 7*, 4379−4381.
10. Rivetti, C., Guthold, M., and Bustamante, C. (1999) Wrapping of DNA around the *E. coli* RNA polymerase open promoter complex, *EMBO J. 18*, 4464−4475.
11. Rippe, K., Guthold, M., von Hippel, P. H., and Bustamante, C. (1997) Transcriptional activation via DNA-looping: Visualization of intermediates in the activation pathway of *E. coli* RNA polymerase × σ54 holoenzyme by scanning force microscopy, *J. Mol. Biol. 270*, 125−138.
12. Bandwar, R. P., and Patel, S. S. (2001) Peculiar 2-aminopurine fluorescence monitors the dynamics of open complex formation by bacteriophage T7 RNA polymerase, *J. Biol. Chem. 276*, 14075−14082.
13. Bandwar, R. P., Jia, Y., Stano, N. M., and Patel, S. S. (2002) Kinetic and thermodynamic basis of promoter strength: Multiple steps of transcription initiation by T7 RNA polymerase are modulated by the promoter sequence, *Biochemistry 41*, 3586−3595.
14. Villemain, J., Guajardo, R., and Sousa, R. (1997) Role of open complex instability in kinetic promoter selection by bacteriophage T7 RNA polymerase, *J. Mol. Biol. 273*, 958−977.
15. Jia, Y., and Patel, S. S. (1997) Kinetic mechanism of GTP binding and RNA synthesis during transcription initiation by bacteriophage T7 RNA polymerase, *J. Biol. Chem. 272*, 30147−30153.
16. Stano, N. M., Levin, M. K., and Patel, S. S. (2002) The +2 NTP binding drives open complex formation in T7 RNA polymerase, *J. Biol. Chem. 277*, 37292−37300.
17. Cheetham, G. M., Jeruzalmi, D., and Steitz, T. A. (1999) Structural basis for initiation of transcription from an RNA polymerase-promoter complex, *Nature 399*, 80−83.
18. Cheetham, G. M., and Steitz, T. A. (1999) Structure of a transcribing T7 RNA polymerase initiation complex, *Science 286*, 2305−2309.
19. Gohlke, C., Murchie, A. I., Lilley, D. M., and Clegg, R. M. (1994) Kinking of DNA and RNA helices by bulged nucleotides observed by fluorescence resonance energy transfer, *Proc. Natl. Acad. Sci. U.S.A. 91*, 11660−11664.
20. Lorenz, M., Hillisch, A., Payet, D., Buttinelli, M., Travers, A., and Diekmann, S. (1999) DNA bending induced by high mobility group proteins studied by fluorescence resonance energy transfer, *Biochemistry 38*, 12150−12158.
21. Parkhurst, L. J., Parkhurst, K. M., Powell, R., Wu, J., and Williams, S. (2001) Time-resolved fluorescence resonance energy transfer studies of DNA bending in double-stranded oligonucleotides and in DNA-protein complexes, *Biopolymers 61*, 180−200.
22. Lorenz, M., Hillisch, A., and Diekmann, S. (2002) Fluorescence resonance energy transfer studies of U-shaped DNA molecules, *J. Biotechnol. 82*, 197−209.
23. Hardwidge, P. R., Wu, J., Williams, S. L., Parkhurst, K. M., Parkhurst, L. J., and Maher, L. J., III (2002) DNA bending by bZIP charge variants: A unified study using electrophoretic phasing and fluorescence resonance energy transfer, *Biochemistry 41*, 7732−7742.
24. King, G. C., Martin, C. T., Pham, T. T., and Coleman, J. E. (1986) Transcription by T7 RNA polymerase is not zinc-dependent and is abolished on amidomethylation of cysteine-347, *Biochemistry 25*, 36−40.
25. Clegg, R. M., Murchie, A. I., Zechel, A., and Lilley, D. M. (1993) Observing the helical geometry of double-stranded DNA in solution by fluorescence resonance energy transfer, *Proc. Natl. Acad. Sci. U.S.A. 90*, 2994−2998.
26. Haugland, R. P., Ed. (2002) *Handbook of Fluorescent Probes and Research Products*, 9th ed., Molecular Probes, Inc., Eugene, OR.
27. Ujvari, A., and Martin, C. T. (1997) Identification of a minimal binding element within the T7 RNA polymerase promoter, *J. Mol. Biol. 273*, 775−781.
28. Tang, G. Q., Bandwar, R. P., and Patel, S. S. (2005) Extended upstream A-T sequence increases T7 promoter strength, *J. Biol. Chem. 280*, 40707−40713.
29. Dietrich, A., Buschmann, V., Muller, C., and Sauer, M. (2002) Fluorescence resonance energy transfer (FRET) and competing processes in donor−acceptor substituted DNA strands: A comparative study of ensemble and single-molecule data, *J. Biotechnol. 82*, 211−231.
30. Martin, C. T., and Coleman, J. E. (1987) Kinetic analysis of T7 RNA polymerase-promoter interactions with small synthetic promoters, *Biochemistry 26*, 2690−2696.
31. Maslak, M., and Martin, C. T. (1993) Kinetic analysis of T7 RNA polymerase transcription initiation from promoters containing single-stranded regions, *Biochemistry 32*, 4281−4285.

32. Bandwar, R. P., and Patel, S. S. (2002) The energetics of consensus promoter opening by T7 RNA polymerase, *J. Mol. Biol. 324*, 63−72.
33. Bhattacharyya, A., and Lilley, D. M. (1989) The contrasting structures of mismatched DNA sequences containing looped-out bases (bulges) and multiple mismatches (bubbles), *Nucleic Acids Res. 17*, 6821−6840.
34. Gaal, T., Bartlett, M. S., Ross, W., Turnbough, C. L., Jr., and Gourse, R. L. (1997) Transcription regulation by initiating NTP concentration: rRNA synthesis in bacteria, *Science 278*, 2092−2097.
35. Place, C., Oddos, J., Buc, H., McAllister, W. T., and Buckle, M. (1999) Studies of contacts between T7 RNA polymerase and its promoter reveal features in common with multisubunit RNA polymerases, *Biochemistry 38*, 4948−4957.
36. Brieba, L. G., and Sousa, R. (2001) The T7 RNA polymerase intercalating hairpin is important for promoter opening during initiation but not for RNA displacement or transcription bubble stability during elongation, *Biochemistry 40*, 3882−3890.
37. Brieba, L. G., and Sousa, R. (2001) T7 promoter release mediated by DNA scrunching, *EMBO J. 20*, 6826−6835.
38. Bloomfield, V. A., Crothers, D. M., and Tinoco, I., Jr. (2000) *Nucleic Acids: Structures, Properties, and Functions*, University Science Books, Sausalito, CA.
39. Bewley, C. A., Gronenborn, A. M., and Clore, G. M. (1998) Minor groove-binding architectural proteins: Structure, function, and DNA recognition, *Annu. Rev. Biophys. Biomol. Struct. 27*, 105−131.
40. Stano, N. M., and Patel, S. S. (2002) The intercalating β-hairpin of T7 RNA polymerase plays a role in promoter DNA melting and in stabilizing the melted DNA for efficient RNA synthesis, *J. Mol. Biol. 315*, 1009−1025.
41. Liu, C., and Martin, C. T. (2002) Promoter clearance by T7 RNA polymerase. Initial bubble collapse and transcript dissociation monitored by base analog fluorescence, *J. Biol. Chem. 277*, 2725−2731.
42. Tang, G.-Q., and Patel, S. S. (2006) Rapid binding of T7 RNA polymerase is followed by simultaneous bending and opening of the promoter DNA, *Biochemistry 45*, 4947−4956.

BI0522910